[Article ID] 1003- 6326(2001)03- 0399- 06

Thermal residual stresses and stress distributions under tensile and compressive loadings of short fiber reinforced metal matrix composites①

DING Xiang-dong(丁向东)[1, 2], LIAN Jian-she(连建设)[2],
JIANG Zhong-hao(江中浩)[2], SUN Jun(孙 军)[1]
(1. State Key Laboratory for Mechanical Behavior of Materials,
School of Materials Science and Engineering,
Xi'an Jiaotong University, Xi'an 710049, P. R. China;
(2. College of Materials Science and Engineering, Jilin University of Technology,
Changchun 130025, P. R. China)

[Abstract] The thermal residual stresses and the stress distributions of short fiber reinforced metal matrix composite under tensile and compressive loadings were studied using large strain axisymmetric elasto-plastic finite element method. It is demonstrated that the thermal residual stresses can result in asymmetrical stress distributions and matrix plasticity. The thermal residual stresses decrease the stress transfer in tension and enhance the stress transfer in compression. The fiber volume fraction has more important effects on the thermal residual stresses and the stress distributions under tensile and compressive loadings than the fiber aspect ratio and the fiber end distance.

[Key words] metal matrix composite; finite element method; thermal residual stresses; stress distribution
[CLC number] TB 331 [Document code] A

1 INTRODUCTION

Due to larger difference in thermal expansion coefficient between the fiber and the matrix and special geometrical shape of the fiber, the thermal residual stresses (TRS) generated during cooling from high (processing) temperature to room temperature have important influences on the mechanical properties of short fiber reinforced metal matrix composites (SFRMMC)[1~8]. To interpret these influences, some investigators used the Eshelby method to calculate the average TRS in the matrix and the fiber and to relate them to the composite properties[1, 2]; another investigators applied the finite element method (FEM) to study the distributions of TRS and their influences on the composite flow curves[3~8]. However, it can be noted that there are only very limited studies about detailed distributions of TRS and the stress distributions under the tensile and compressive loadings and the effects of the material parameters on stress distributions. Therefore, in the present study, the large strain axisymmetric elasto-plastic FEM is used to investigate the effects of the material structure parameters (fiber volume fraction, fiber aspect ratio and fiber end distance) on the distributions of TRS and subsequent stress distributions under the tensile and compressive loadings of typical SiC whisker reinforced aluminum matrix composite.

2 FINITE ELEMENT MODEL

Two geometric models, one with the fiber ends aligned and the other with them staggered, were in general used for the typical FEM calculation of MMCs. For SiC_w/6061Al composite here, according to the results of experiment[4, 5], the aligned model was used. The composite was assumed to consist of an array of hexagonal unit cells, each unit cell contains a cylindrical fiber. The unit cell is further regarded as a cylindrical unit cell, as shown in Fig. 1(a).

The fiber volume fraction is written as

$$\varphi_F = (\pi R_F^2 L_F)/(\pi R_C^2 L_C) \quad (1)$$

And the aspect ratios of the fiber and the unit cell are defined as

$$A_F = L_F/R_F,\ A_C = L_C/R_C \quad (2)$$

The fiber end distance is described as

$$K = L_C/L_F \quad (3)$$

where R_F and L_F, R_C and L_C are the radius and the lengths of the fiber and the unit cell, respectively.

Due to the symmetry of the model, only quarter of the unit cell is considered in the present analysis. 4-Crossed Triangle Element is used, the finite element mesh is identical to that in Ref. [9]. The total numbers of the nodes and the quadrilateral elements are 2045 and 980, respectively.

The loading history of the composite was as

① [Foundation item] Project (59625102) supported by the National Outstanding Youth Foundation of China
[Received date] 2000- 07- 28; [Accepted date] 2000- 12- 20

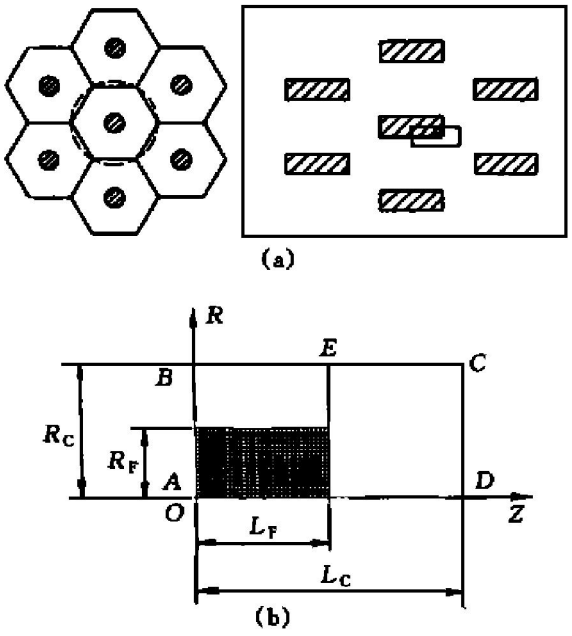

Fig. 1 Schematic diagram of fiber arrangement in composite (a) and boundary condition in FEM (b)

follows.

1) A thermal loading was applied to the composite to calculate thermal residual stresses generated during cooling from processing (high) temperature to room (low) temperature. The boundary conditions for this step are shown in Fig. 1(b).

in AD $u_R = 0$, $T_Z = 0$;

in AB $u_Z = 0$, $T_R = 0$;

in DC $u_Z = U_1$; $\int_0^{R_C} T_Z R \mathrm{d}R = 0$, $T_R = 0$;

in BC, $\int_0^{L_C} T_R \mathrm{d}Z = 0$, $T_Z = 0$, $u_R = U_2$

where u_Z, u_R and T_Z, T_R are the displacement rates and the loading rates of the unit cell boundaries along the Z and R directions; U_1 and U_2 are the uniform displacement rates in the unit cell boundaries, which should keep uniform during the simulation.

2) A tensile or compressive loading was applied to the composite at room temperature to calculate respectively the stress distribution in two loading conditions.

in AD, AB and BC, same as thermal loading;

in DC, $T_R = 0$, $u_Z = U$

where U is the prescribed axial displacement rate.

The analysis assumes that the fiber was a linear elastic material and the matrix was a linear elastic thermo-plastic material exhibiting isotropic work hardening and obeying the von Mises yield criterion. Furthermore, the analysis assumed that a perfect interfacial bound existed between the fiber and the matrix. The updated-Lagrangian-Jaumann formulation, the J_2F flow theory of thermal elastic-plastic, the virtual power equilibrium equation and the element stiffness equation described by Lagrange stress tensor[10] were used in the finite element calculations.

Since TRS in most SFRMMCs, e. g. SiC_w/6061Al composites, are generated mainly at a lower temperature interval above room temperature and the material parameters (the elastic moduli, Poisson's ratios and the coefficients of thermal expansion of the matrix and the fiber, E_M, E_F, υ_M, υ_F, α_M and α_F) are generally insensitive to temperature[4, 7, 8, 11], they are approximately assumed to be independent of temperature. In the present calculations, these material parameters are taken from a typical SiC whisker reinforced aluminum matrix composite (SiC_w/6061Al, T6 heat-treatment)[2, 11, 12], i. e. $E_M = 74$ GPa, $E_F = 483$ GPa, $\upsilon_M = 0.33$, $\upsilon_F = 0.17$, $\alpha_M = 23 \times 10^{-6}$/℃ and $\alpha_F = 4.31 \times 10^{-6}$/℃; the yield strength and the work hardening ratio of the matrix $\sigma_M = 357$ MPa and $n = 0.20$; the temperature change is chosen as $|\Delta\theta| = 200$ ℃.

3 RESULTS AND DISCUSSION

3.1 Distributions of TRS

Fig. 2 shows the distributions of the matrix axial residual stress σ_M^R, the fiber axial residual stress σ_F^R (averaging over the cross-sections of the matrix and the fiber, respectively) and the interfacial residual

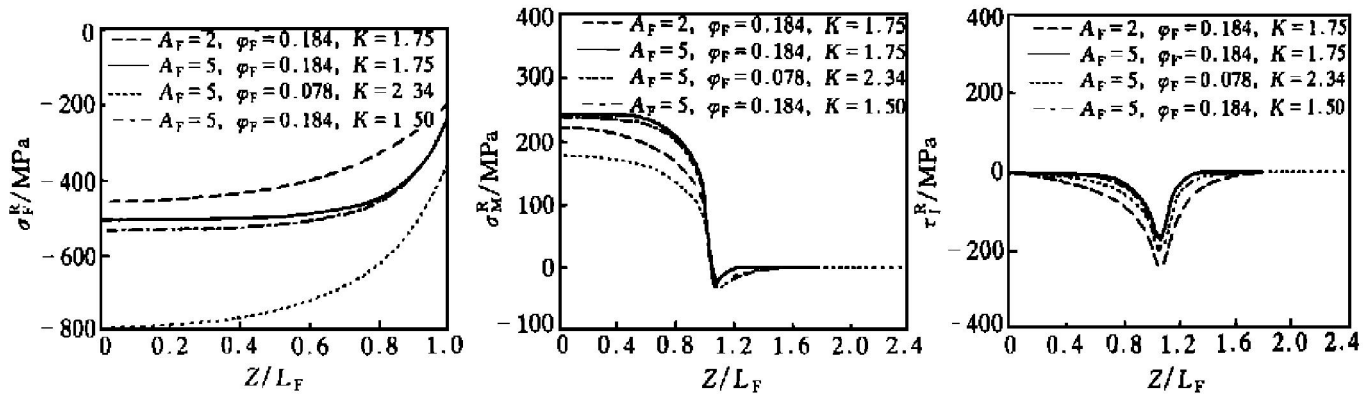

Fig. 2 Distributions of fiber axial residual stress (σ_F^R), matrix axial residual stress (σ_M^R) and interfacial shear residual stress (τ_I^R)

shear stress τ_I^R (along the matrix-fiber interface, i. e. at $R = R_F$) for different fiber volume fraction φ_F, fiber aspect ratio A_F and fiber end distance K (the calculations show that the distributions of the above residual stresses are non-uniform in the radial or R direction). Fig. 2 shows that the distributions of σ_M^R, σ_F^R and τ_I^R are non-uniform along the fiber direction. In the fiber region ($0 \leqslant Z \leqslant L_F$), σ_M^R is tensile (positive value) and σ_F^R is compressive (negative value). σ_M^R and σ_F^R have their maximum (absolute) values in the middle section of the unit cell ($Z = 0$). σ_M^R is equal to zero in most of the fiber end region ($L_F \leqslant Z \leqslant L_C$) and σ_M^R is smaller than zero in a small region near the fiber end face ($Z = L_F$), indicating that the fiber end face endures a compressive stress. τ_I^R (absolute value is zero at $Z = 0$ and $Z = L_C$, and has its maximum (absolute) value at $Z = L_F$.

Fig. 2 also shows that φ_F, A_F and K have important effects on the distributions of σ_M^R, σ_F^R and τ_I^R. σ_M^R increases, σ_F^R (absolute value) decreases and τ_I^R has small variation with the increase of φ_F. σ_M^R and σ_F^R (absolute value) increase and τ_I^R decreases with increase of A_F. σ_M^R increases, σ_F^R (absolute value) decreases and τ_{RZ}^R has small variation with the increase of K. It can be seen from Fig. 2 that φ_F has larger effects on σ_M^R and σ_F^R than A_F and K. φ_F, A_F and K have relatively small effects on τ_I^R.

3.2 Development of matrix plasticity

To study the development of the matrix plasticity, the contours of the von Mises effective stress and the hydrostatic stress in the matrix and the fiber under tensile and compressive loadings for $A_F = A_C = 5$, $\varphi_F = 0.184$ and $K = 1.75$ (for this K value, $L_F/L_C = R_F/R_C$[4, 8]) are given in Fig. 3 and Fig. 4. Fig. 3 shows that in the fiber region, the effective stress in the matrix is very high when the tensile or compressive strain is equal to zero, the plastic deformation occurs in a thin layer region around the fiber. In the fiber end region, the effective stress in the matrix is relatively lower and the plastic deformation occurs only in local region near the fiber sharp corner. Fig. 4 reveals that the distributions of the hydrostatic stress

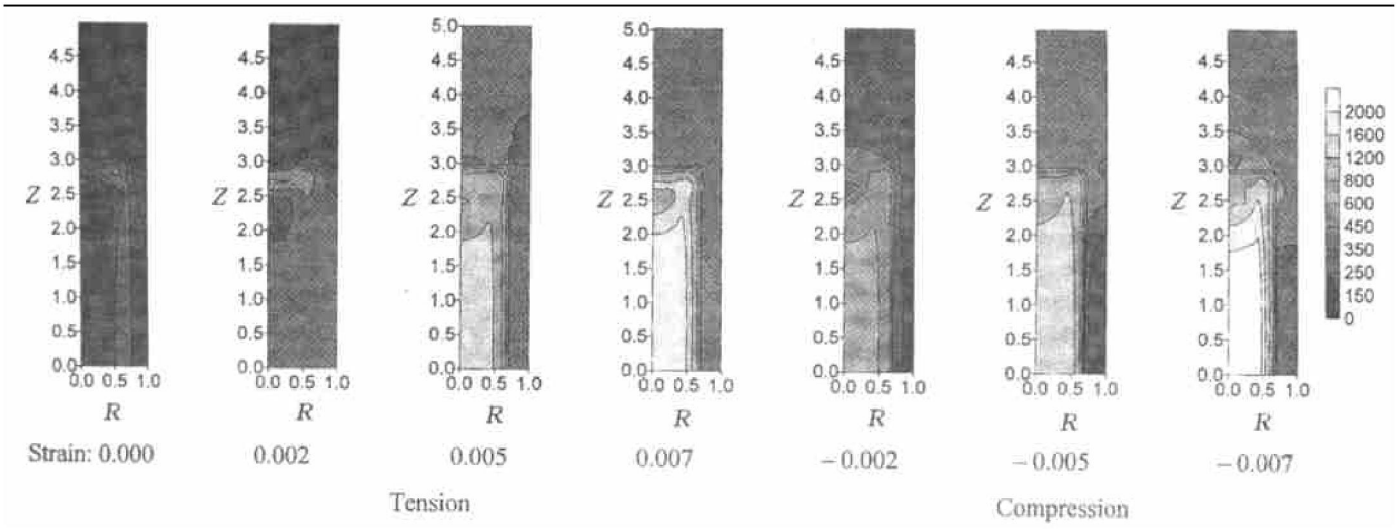

Fig. 3 Contours of von Mises effective stress of matrix and fiber in tension and compression

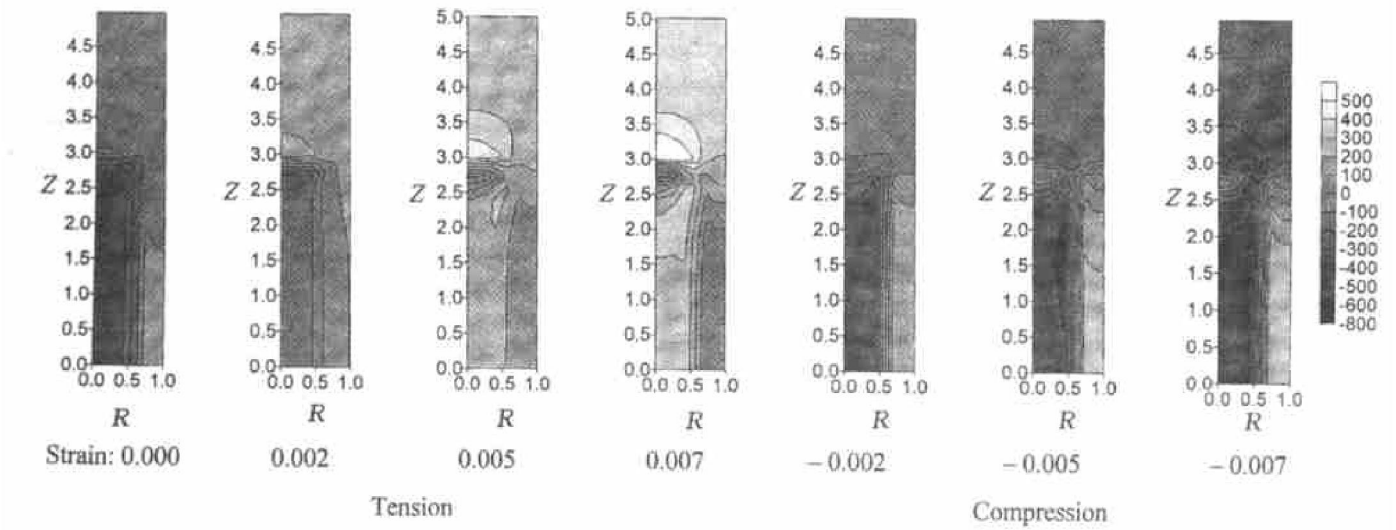

Fig. 4 Contours of hydrostatic stresses in matrix and fiber in tension and compression

are non-uniform in the matrix and fiber, especially in the region around the fiber end face. The entire fiber is in a state of hydrostatic compression, the entire matrix is in a state of the hydrostatic tension.

When a tensile loading is applied to the composite, the plastic deformation in the matrix develops rapidly in the fiber region and the matrix in this region enters a plastic state at a very small strain (ε_C= 0.002). Because the effective TRS is lower before the tensile loading, the plastic deformation occurs in the fiber end region, most of the matrix in this region enters the plastic state at a larger strain (ε_C = 0.005). The calculations reveal that when the tensile strain reaches 0.006 4, the entire matrix in the fiber region and the fiber end region enter a full plastic state. Fig. 4 shows that as the applied tensile strain increases, there is a transition of the stress state in the fiber from hydrostatic compression to hydrostatic tension. This transition is slower and a hydrostatic compressive region exists still in the fiber near the fiber end face at ε_C = 0.007. In the fiber region, there is a transition of the stress state in the matrix from hydrostatic tension to hydrostatic compression. As the tensile strain increases, the hydrostatic tensile stress in the matrix decreases, but there is still a hydrostatic compressive region near the middle section of the unit cell at ε_C= 0.007. In the fiber end region, the hydrostatic tensile stress in the matrix increases with increasing the tensile strain and is the largest in the region near the fiber end face.

When a compressive loading is applied to the composite, the effective TRS in the fiber increases with increasing compressive strain. In the fiber region, the effective stress in the matrix first decreases when the compressive strain is smaller ($\varepsilon_C \leqslant$0.002), then increases slowly. In the fiber end region, the effective stress in the matrix near the fiber end face increases quickly, and the plastic region extends toward the region far from the fiber end face. The distributions of the effective stress in Fig. 3 reveal that in compression, the matrix enters a full plastic state when the compressive strain reaches − 0.010, which (absolute value) is larger than that in tension (ε_C= 0.006 4). It can be seen from the distribution of the hydrostatic stress in Fig. 4 that there is a transition of the stress state in the matrix from the hydrostatic tension to the hydrostatic compression during the compressive loading.

3.3 Stress distributions under tensile and compressive loadings

The distributions of the matrix axial stresses σ_M (averaging over the fiber cross-section), the fiber axial stresses σ_F (averaging over the fiber cross-section) and the interfacial shear stress τ_I (along the matrix-fiber interface) are shown in Fig. 5 for given φ_F, A_F and K. In tension, as the tensile strain increases, σ_F (absolute value) decreases and becomes tensile, the gradient of σ_F along the fiber direction has a reverse change. In the fiber region, σ_M increases first, then decreases with increasing the tensile strain. In the fiber end region, σ_M increases continuously with increasing applied tensile strain and is larger than that

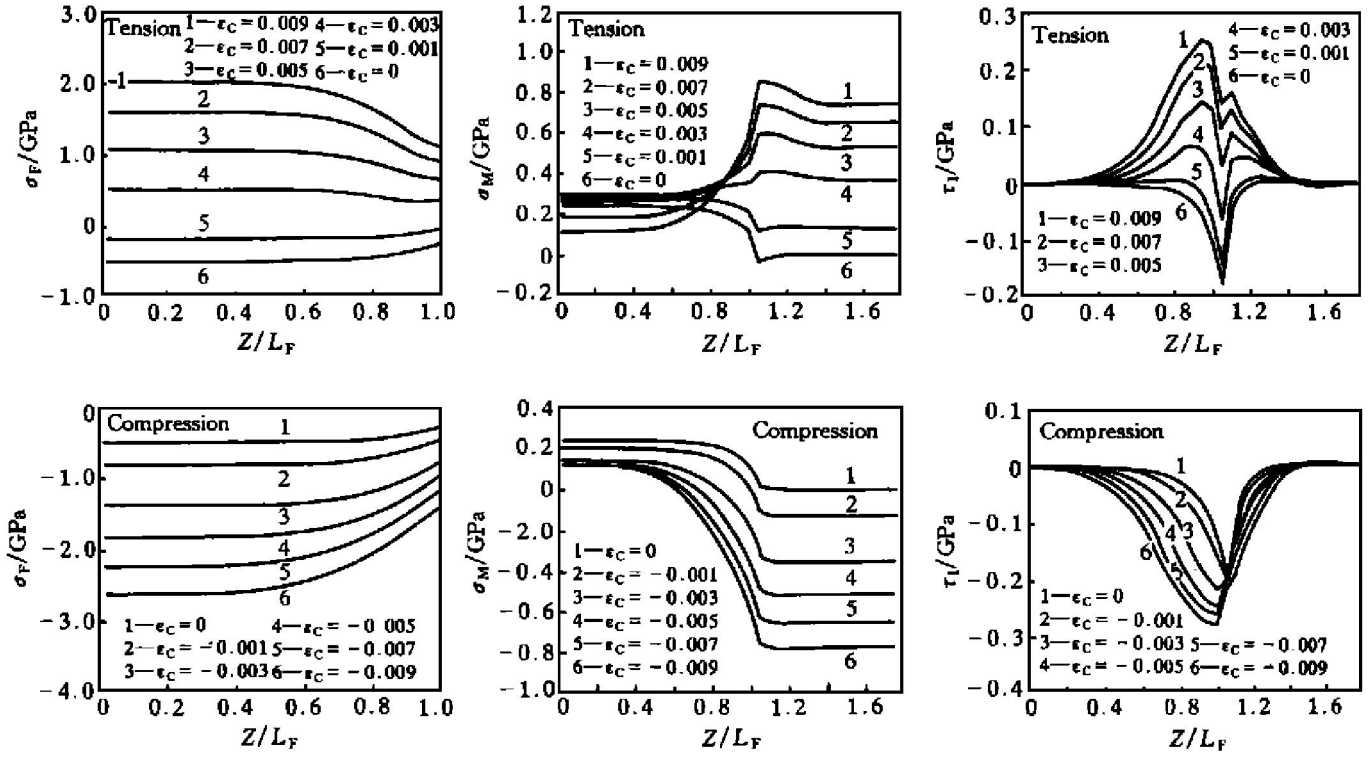

Fig. 5 Distributions of fiber axial stress (σ_F), matrix axial stress (σ_M) and interfacial shear stress (τ_I) under tensile and compressive loadings

in the fiber region. In the region near the fiber end face, σ_M has a complicated variation. In the entire length of the unit cell, τ_I (absolute value) decreases first and becomes positive, then increases with increasing the tensile strain.

In compression, as the compressive strain increases, σ_F (absolute value) increases. In the fiber region, σ_M decreases and has a transition from tension to compression with increasing the compressive strain. The transition is slow, the local region of the matrix in the middle section of the unit cell is still tensile when the compressive strain is equal to 0.009. In the fiber end region, σ_M increases continuously with increasing the compressive strain. In the entire length of the unit cell, τ_I (absolute value) increases continuously with increasing the compressive strain.

It can be seen from Fig. 5 that due to the presence of TRS, the stress distributions is asymmetrical in tension and compression. The calculations also reveal that at a higher strain level, the average values of the matrix axial stress over the entire matrix in tension is larger than that in compression, while the average values of the fiber axial stress over the entire fiber in compression is larger than that in tension. The latter indicates that the stress transfer effect from the matrix to the fiber in compression is enhanced due to the presence of TRS. Furthermore, it can be found by comparing the results in the absence of TRS[9] with that in the presence of TRS, the stress transfer in tension is smaller than that in the absence of TRS, and the stress transfer in compression is larger than that in the absence of TRS. These changes in the stress transfers (or the fiber axial stress) and the matrix axial stress in tension and compression will produce important influences on the composite properties.

3.4 Effects of material structure parameters

Fig. 6 shows the effects of the material structure parameters φ_F, A_F and K on the stress distributions under tensile or compressive loadings for a given strain (absolute value) of $|\varepsilon_C| = 0.005$. As shown in Fig. 6, the effects of these material structure parameters on the stress distributions are different in tension and compression. As φ_F increases, σ_F in tension increases, σ_F (absolute value) in compression decreases; in the fiber region, σ_M in tension decreases and σ_M in compression increases; while in the fiber end region, σ_M in tension and compression has reverse or same variations to those in the fiber region. τ_I in tension and compression has similar varying tendencies to that with φ_F. In two cases, in most regions near the middle section of the unit cell and the end face of the unit cell, τ_I decreases with increasing φ_F. τ_I in tension has a complicated variation with φ_F in the region near the fiber end face. As A_F increases, in tension and compression, σ_F and σ_M in the fiber region increase, σ_M in the fiber end region increase. The varying tendency

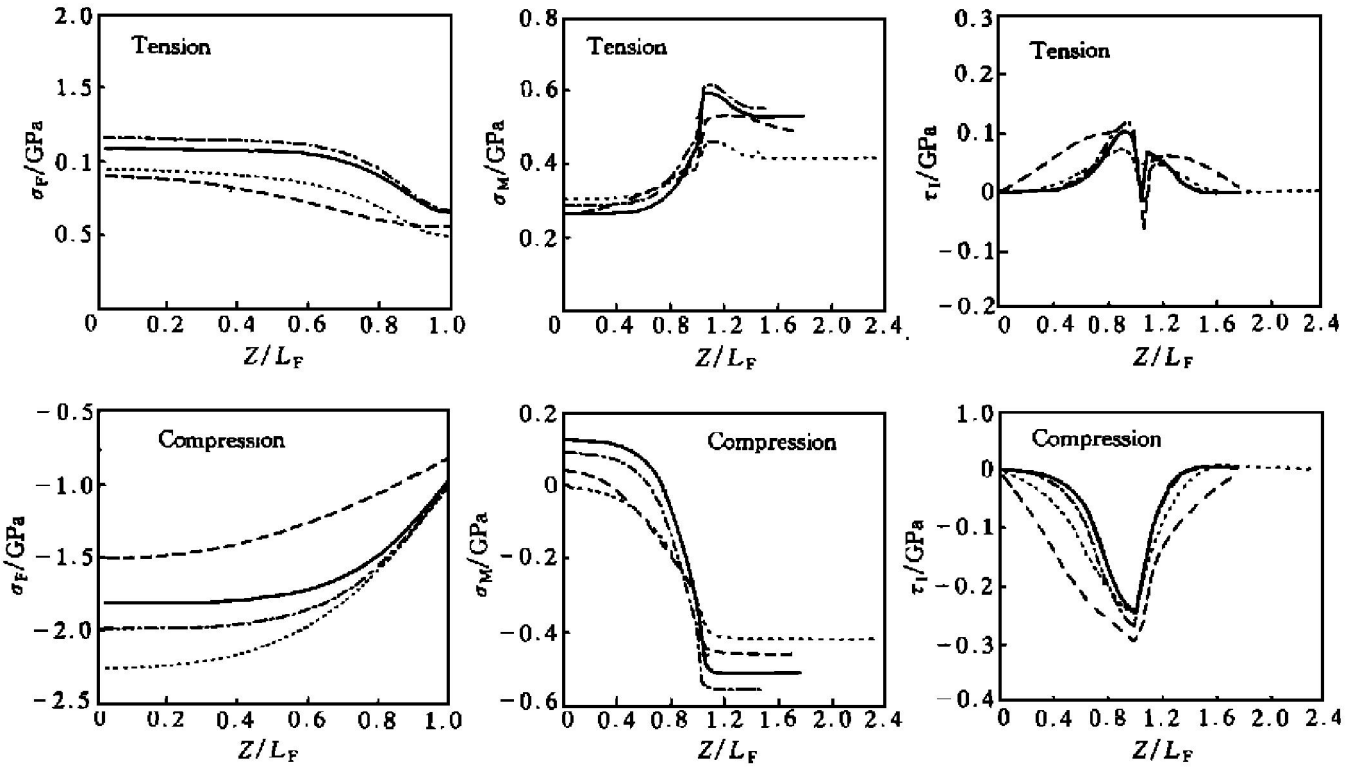

Fig. 6 Effects of the material structure parameters on fiber axial stress (σ_F), matrix axial stress (σ_M) and interfacial shear stress (τ_I) under tensile and compressive loadings

(– – – For $A_F = 2$, $\varphi_F = 0.185$, $K = 1.75$; ——For $A_F = 5$, $\varphi_F = 0.185$, $K = 1.75$; ----- For $A_F = 5$, $\varphi_F = 0.078$, $K = 2.34$; – · – For $A_F = 5$, $\varphi_F = 0.185$, $K = 1.50$)

of τ_I with A_F is similar to that with φ_F. As K decreases, σ_F (absolute value) in tension and compression increases; in compression, σ_M (absolute value) decreases in the fiber region and increases in the fiber end region; while σ_M in tension increases in the both regions. (in compression and tension, τ_I has very small variation in the both regions).

The effects of above three structure parameters on the stress distributions result from mainly two mechanisms, i. e. the stress transfer from the matrix to the fiber and the restraint to deformation between the matrix and the fiber, which originate from the mismatch in the material properties between the matrix and the fiber. The above three structure parameters affect these two mechanisms in different ways and these effects become more complicated due to the presence of TRS. A_F affects mainly the stress transfer by changing the matrix-fiber interfacial length. φ_F affects the stress transfer and also changes the restraint between the matrix and the fiber by partitioning the deformation (the stress and the strain) between the matrix and the fiber. The effects of K on two mechanisms are similar to those of φ_F, but mainly by partitioning the deformation between the fiber region and the fiber end region.

4 CONCLUSIONS

1) The thermal residual stresses in the matrix and the fiber can reach quite high level and distribute non-uniformly. They can result in local plastic deformation in the matrix near the fiber end face and the matrix-fiber interface. The amount and distributions of the thermal residual stresses depend strongly on the material structure parameters. The effect of the fiber volume fraction is more significant than that of the fiber aspect ratio and the fiber end distance.

2) Due to the thermal residual stresses, the stress distributions in the matrix and the fiber and the development of the matrix plasticity are asymmetric under tensile and compressive loadings. In tension, there is a transition of the fiber axial stress from compression to tension, and in compression there is a transition of the matrix axial stress from tension to compression. The thermal residual stresses enhance the stress transfer in compression and reduce the stress transfer in tension compared with that in the absence of the thermal residual stresses.

3) The material structure parameters have important effects on the stress distributions under tensile and compressive loadings. They affect the stress distributions mainly through the effects on the stress transfer and the restraints to the deformation between the matrix and the fiber in different ways. These effects become more complicated due to the presence of the thermal residual stresses.

[REFERENCES]

[1] Withers P J, Stobbs W M, Pedersen O B. The application of the Eshelby method of internal stress determination to short fiber metal matrix composites [J]. Acta Metall, 1989, 37: 3061- 3084.

[2] Taya M, Arsenault R J. A comparison between a shear lag model and an Eshelby type model in predicting the mechanical properties of a short fiber composite [J]. Scripta Metall. 1987, 21: 349- 354.

[3] Povirk G L, Stout M G, Bourke M, et al. Thermally and mechanically induced residual strains in Al-SiC composites [J]. Acta Metall Mater, 1992, 40: 2391- 2412.

[4] Dutta I, Sims J D, Seigenhaler D M. An analytical study of residual stress effects on uniaxial deformation of whisker reinforced metal matrix composites [J]. Acta Metall Mater, 1993, 41: 885- 908.

[5] Jain M, Macewen S R, Wu L. Finite element modeling of residual stresses and strength differential effect in discontinuously reinforced metal matrix composites [J]. Mat Sci Eng, 1994, A183: 111- 120.

[6] Shi N, Arsenault R J, Karwitz A D, et al. Deformation-induced residual stress changes SiC whisker-reinforced 6061Al composites [J]. Metall Trans, 1993, 24A: 187 - 196.

[7] Levy A, Papaziam J M. Elastoplastic finite element analysis of short-fiber-reinforced SiC/Al composites [J]. Acta Metall Mater, 1991, 39: 2255- 2266.

[8] JIANG Z H, LIAN J S, YANG D Z, et al. An analytical study of the influence of thermal residual stresses on the elastic and yield behaviors of short fiber-reinforced metal matrix composites [J]. Mater Sci Eng, 1998, A248: 256- 275.

[9] DING Xiang-dong, LIAN Jian-she, JIANG Zhong-hao, et al. Finite element numerical analysis of tensile stress field in short fiber reinforced metal matrix composite [J]. Acta Metallurgica Sinica, 2000(2): 196- 200.

[10] HU P, LI Y X, LIU Y Q. Numerical Elasto-plastic Mechanics [M]. Changchun: Jilin Science and Technology Publishing House, 1995. 184- 192.

[11] Nardone V C and Prewo K M. On the strength of discontinuous silicon carbide reinforced aluminum alloys [J]. Scripta Metall, 1986, 20: 43- 48.

[12] LI Z H, Schmauder S, Wanner A, et al. Expressions to characterize the flow behavior of particle-reinforced composites based on axisymmetric unit cell models [J]. Scripta Metall Mater, 1995, 33: 1289- 1294.

(Edited by YANG Bing)